Enhanced Low-Temperature Hydrogen Storage in Nanoporous Ni-Based Alloy Supported LiBH$_4$

Xi Chen, Zhao Li, Yue Zhang, Dongming Liu*, Chunyang Wang, Yongtao Li, Tingzhi Si and Qingan Zhang

School of Materials Science and Engineering, Anhui University of Technology, Maanshan, China

To reveal the synergistic effect of nanoconfinement and metallic catalysis on the hydrogen storage properties of LiBH$_4$, the nanoporous Ni-based alloy (np-Ni) was prepared herein by dealloying of the Mn$_{70}$Ni$_{30}$ alloy in (NH$_4$)$_2$SO$_4$ solution, and then LiBH$_4$ was loaded into np-Ni to construct the LiBH$_4$/np-Ni hydrogen storage system using wet impregnation. It was found that dehydrogenation of the LiBH$_4$/np-Ni (1:5) system starts at around 70°C and ends before 400°C, with ~11.9 wt.% of hydrogen desorbed. The apparent dehydrogenation activation energy for the LiBH$_4$/np-Ni (1:5) system was remarkable decreased to about 11.4 kJ/mol. After rehydrogenation at 450°C under 8 MPa hydrogen pressure, ~8.2 wt.% of hydrogen can be released from about 60°C upon second dehydrogenation. These obtained results would provide an efficient strategy for improving the hydrogen storage properties of other metal borohydrides.

Keywords: hydrogen storage, lithium borohydride, nanoporous metal, nanoconfinement, catalysis

INTRODUCTION

Nowadays, the issue of energy shortage has been called into public focus. Hydrogen is considered to be the most ideal secondary source because of its high calorific value, low environmental impact and abundant resources (Abe et al., 2019). To meet the need of storing hydrogen with high efficiency and safety, it is necessary to develop hydrogen storage materials with high mass and volume hydrogen density (Yang et al., 2010; Li H. W. et al., 2011; Abdalla et al., 2018). LiBH$_4$ has attracted much more attention due to its extremely high theoretical hydrogen storage capacity of 18.5 wt.%. However, the elevated dehydrogenation temperature, complicated dehydrogenation behavior and poor reversibility limit its practical applications (Züttel et al., 2003; Orimo et al., 2005; Mauron et al., 2008; Li C. et al., 2011). In order to overcome these deficiencies, the strategies of constructing reactive hydride system (Liu D. M. et al., 2013; Liu et al., 2015, 2016; Ding et al., 2019), cation/anion substitution (Yin et al., 2008; Fang et al., 2011), adding catalyst (Zhang et al., 2017; Cai et al., 2018) and nanoconfinement (Guo et al., 2017; Xu et al., 2017; Meng et al., 2018) were developed in the last decade.

Nanoconfinement of LiBH$_4$ in nanoporous material can maintain the particle within a nanoscale structure, which is exceedingly beneficial to enlarge the reaction interface and shorten the element diffusion distance, thus significantly enhancing the de-/rehydrogenation properties (Ngene et al., 2010b; Shao et al., 2015; Meng et al., 2018; Gasnier et al., 2019). For example, Zhang et al. found that LiBH$_4$ nanoparticles supported by disordered mesoporous carbon (CMK-3) showed a single dehydrogenation peak at about 332°C and a large dehydrogenation amount of 14 wt.% below 600°C (Zhang et al., 2007). Fang et al. embedded LiBH$_4$ into active carbon (AC) by chemical impregnation.

Due to the enhancement of both the thermodynamic and kinetic properties, the LiBH$_4$/AC system began to release hydrogen at 220°C, which is 150°C lower than bulk LiBH$_4$ without nanostructure modulation (Fang et al., 2008b). Other nanoporous material scaffolds, such as carbon aerogel (Zhao et al., 2014; Surrey et al., 2016), ordered mesoporous carbon (Cai et al., 2016), metallic organic framework (MOFs) (Sun et al., 2011) and mesoporous silicon dioxide (SBA-15) (Ngene et al., 2010a), were also used as the confinement carriers to support LiBH$_4$.

However, the above reported nanoconfinement carriers are composed of non-metallic material that can only provide a single nanoconfinement role for LiBH$_4$ in general. Taking into account that transition metal elements (e.g., Ni and Co) can serve as the active catalyst in improving the hydrogen storage properties of complex hydrides owing to their high electronegativity0 (Ngene et al., 2011; Liu et al., 2018; Zhang et al., 2018), a synergistic effect of nanoconfinement and catalysis would be achieved by confining LiBH$_4$ in nanoporous transition metal. Based on this consideration, nanoporous Ni-based alloy was prepared by dealloying of the Mn$_{70}$Ni$_{30}$ alloy and then used as the carrier to support LiBH$_4$ in this work, and a significantly improved low-temperature hydrogen storage in LiBH$_4$ was successfully obtained.

EXPERIMENTAL SECTION

Sample Preparation

Commercial LiBH$_4$ powder (95%, Alfa Aesar), Mn bulk (99.5%, Alfa Aesar), Ni sheet (99.5%, Alfa Aesar) and tetrahydrofuran (THF) (99.8%, anhydrous, Alfa Aesar) were used in experiments. The Mn$_{70}$Ni$_{30}$ alloy was prepared by induction melting of appropriate amounts of Mn and Ni metals. For compensating the loss of Mn during melting, the extra 3 wt.% of Mn was added on the basis of stoichiometric amount. The as-cast Mn$_{70}$Ni$_{30}$ alloy was mechanically crushed into powders of 200 mesh, and the nanoporous Ni-based alloy (denoted as np-Ni) was prepared by dealloying of the Mn$_{70}$Ni$_{30}$ alloy powders in 1 mol/L (NH$_4$)$_2$SO$_4$ solution at 50°C for 2 h. The LiBH$_4$/np-Ni (1:5) system was prepared by loading LiBH$_4$ into np-Ni using wet impregnation method. Firstly, LiBH$_4$ was dissolved in anhydrous THF. Then,

np-Ni was put in the LiBH$_4$ solution according to the LiBH$_4$/np-Ni weight ratio of 1:5. Finally, the mixture was evacuated for 24 h to remove THF solvent.

Sample Characterization

De-/rehydrogenation properties were examined based on the volumetric method by using a carefully calibrated Sieverts-type apparatus. Thermal dehydrogenation was performed by heating the sample from ambient temperature to 500°C at a rate of 2°C/min. Isothermal dehydogenation was performed by quickly heating and then keeping the sample at a given temperature. The hydrogen back pressure for the above temperature ramp and isothermal dehydrogenation examinations was below 0.1 MPa. Isothermal rehydrogenation was carried out at 450°C under 8 MPa hydrogen pressure. The weight of np-Ni was not taken into account in calculating the hydrogen de-/absorption amounts.

X-ray diffraction (XRD) measurement was performed by a Rigaku D/Max 2500VL/PC diffractometer at 50 kV and 200 mA with Cu Kα radiation. A special Ar-filled holder was applied to seal the XRD sample to avoid contact with air in the course of measurement. To quantitatively investigate the phase structure change of the Mn$_{70}$Ni$_{30}$ alloy before and after dealloying, the XRD profiles were analyzed with the Rietveld refinement program RIETAN-2000 (Izumi and Ikeda, 2000). Scanning electron microscopy (SEM) was carried out using a Nova NanoSEM 430 microscope equipped with an energy dispersive X-ray spectrometer (EDS). Transmission electron microscopy (TEM) observation was performed on a JEM-2100F instrument. Pore size distribution, pore volume and specific surface area were determined by a Micromeritics ASAP 2020 fully-automatic analyzer based on the Brunauer–Emmett–Teller (BET) and Barrett–Joyner–Halenda (BJH) methods (Lowell et al., 2004). Fourier transform infrared (FTIR) spectrum was collected using a Nicolet 6700 FTIR spectrometer.

RESULTS AND DISCUSSION

Structural Analysis of LiBH$_4$/np-Ni System

Figure 1 gives the observed XRD patterns and the Rietveld analysis results of Mn$_{70}$Ni$_{30}$ alloy before and after dealloying, and the phase abundances and structural parameters refined by
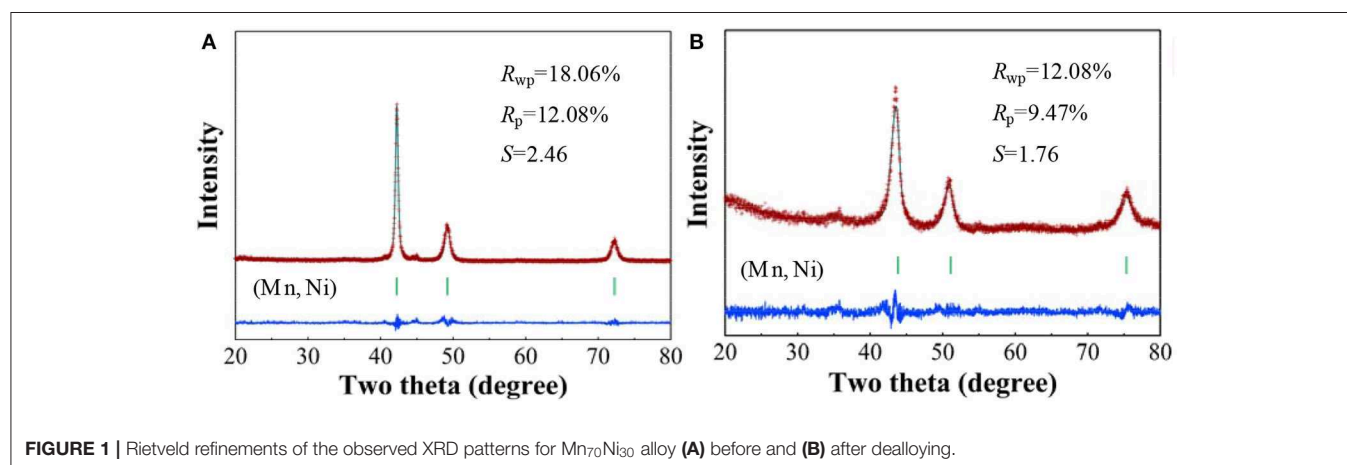
FIGURE 1 | Rietveld refinements of the observed XRD patterns for Mn$_{70}$Ni$_{30}$ alloy **(A)** before and **(B)** after dealloying.

the Rietveld analysis are listed in **Table 1**. It can be seen that the Mn$_{70}$Ni$_{30}$ alloy before and after dealloying are both composed of a single phase of (Mn, Ni) solid solution with a Cu-type structure. However, the XRD peaks of np-Ni are relatively broadened and move toward higher angle as compared with the Mn$_{70}$Ni$_{30}$ alloy. The results indicate that the grain size and cell parameters of the sample were both decreased with the extraction of Mn atom from (Mn, Ni) solid solution upon dealloying due to that Mn has a larger atomic radius relative to Ni.

TABLE 1 | Phase components and structural parameters of Mn$_{70}$Ni$_{30}$ alloy and np-Ni.

Sample	Phase	Space group	Lattice parameters (Å)			Abundance (%)
			a	**b**	**c**	
Mn$_{70}$Ni$_{30}$ alloy	(Mn, Ni)	*Fm-3m*	3.6907(2)	3.6907(2)	3.6907(2)	100
np-Ni	(Mn, Ni)	*Fm-3m*	3.5601(1)	3.5601(1)	3.5601(1)	100

Figure 2 presents the SEM images and corresponding EDS spectra of Mn$_{70}$Ni$_{30}$ alloy and np-Ni. As seen from **Figure 2A**, the Mn$_{70}$Ni$_{30}$ alloy has a smooth surface with a particle size of about ∼70 μm. The EDS result (see **Figure 2C**) indicates that it consists of 70.22 at.% Mn and 29.78 at.% Ni, agreeing well with its nominal element composition. For np-Ni, as given in **Figure 2D**, the element content of Mn is decreased to 21.09 at.%. It is reasonably considered that the massive lixiviation of Mn atom can bring large lattice distortion and physical shrinkage stress, thus leading to the formation of a nanoporous structure as shown in **Figure 2B**.

Figure 3A demonstrates the N$_2$ adsorption/desorption isotherms for np-Ni and the LiBH$_4$/np-Ni (1:5) system. It can be seen that np-Ni has a typical IV-type adsorption isotherm with an obvious hysteresis loop. Those are the characteristics of mesoporous material. In comparison, the hysteresis loop has almost disappeared for the LiBH$_4$/np-Ni (1:5) system. The pore size distributions of np-Ni and the LiBH$_4$/np-Ni (1:5) system are compared in **Figure 3B**, which indicates that the peak in pore size distribution of np-Ni moves to a lower position with
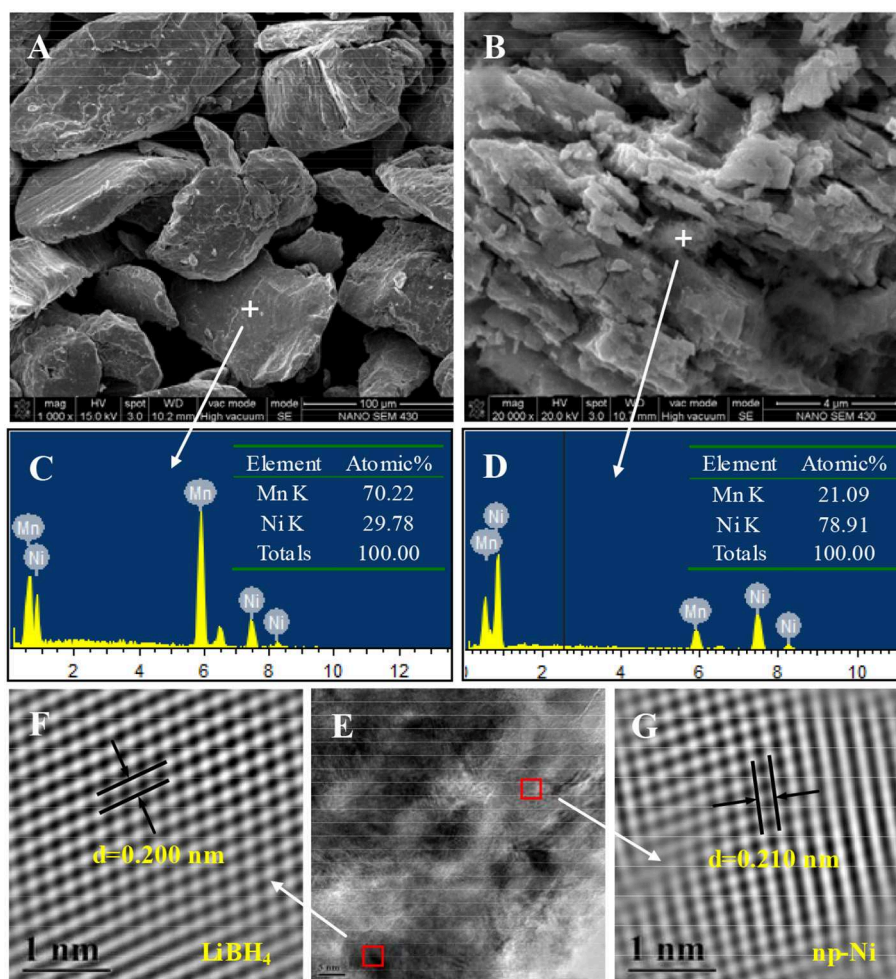
FIGURE 2 | SEM images and EDS spectra of **(A,C)** Mn$_{70}$Ni$_{30}$ alloy and **(B,D)** np-Ni; **(E)** TEM micrograph of the LiBH$_4$/np-Ni (1:5) system and **(F,G)** atomic lattice images of the square regions in **(E)**.
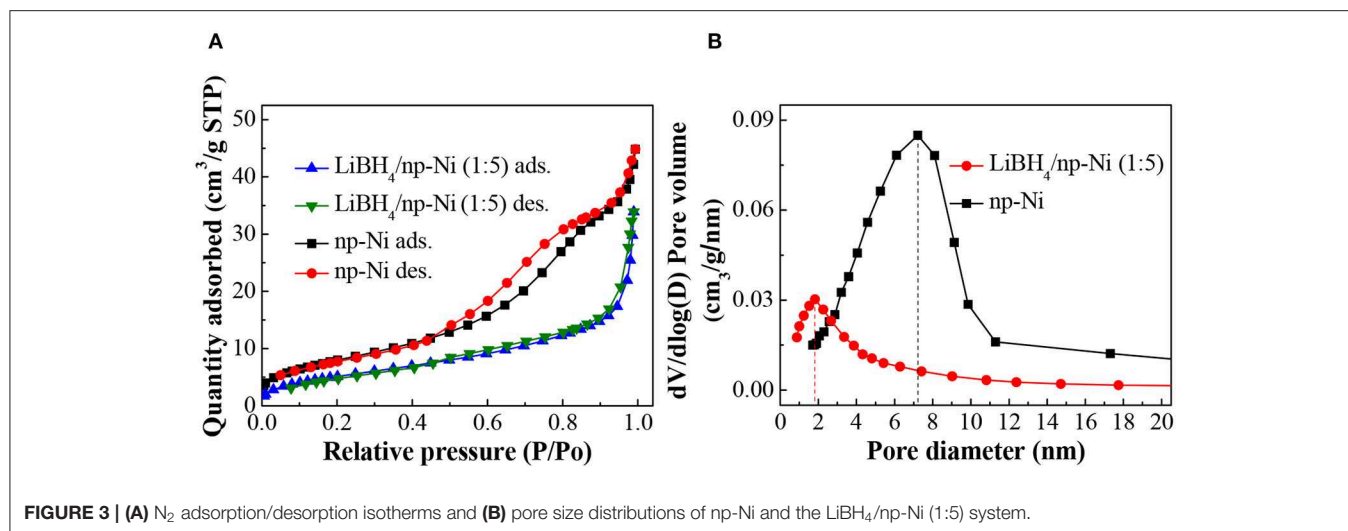
FIGURE 3 | **(A)** N$_2$ adsorption/desorption isotherms and **(B)** pore size distributions of np-Ni and the LiBH$_4$/np-Ni (1:5) system.

TABLE 2 | Pore parameters and specific surface area of np-Ni and the LiBH$_4$/np-Ni (1:5) system.

Sample	Pore size (nm)	Pore volume (cm^3/g)	Specific surface area (m^2/g)
np-Ni	7.21	0.0586	155
LiBH$_4$/np-Ni	1.80	0.0339	17

an intensive decline in intensity after supporting LiBH$_4$. **Table 2** gives the pore parameters and specific surface area of np-Ni and the LiBH$_4$/np-Ni (1:5) system. It is observed that np-Ni has the pore diameter, pore volume and specific surface area of 7.21 nm, 0.0586 cm^3/g and 155 m^2/g, respectively. However, those values reduce to 1.80 nm, 0.0339 cm^3/g and 17 m^2/g, respectively, for the LiBH$_4$/np-Ni (1:5) system. These results imply that LiBH$_4$ was loaded on the surface and impregnated into the pores of np-Ni. **Figure 2E** gives the TEM micrograph of the LiBH$_4$/np-Ni (1:5) system, and **Figures 2F,G** present the atomic lattice images of the square regions in **Figure 2E** obtained by inverse fast Fourier transform (IFFT). The fringe spacings of 0.200 nm in **Figure 2F** and 0.210 nm in **Figure 2G** correspond to (121) plane of LiBH$_4$ and (111) plane of Ni, respectively. The TEM results reveal that LiBH$_4$ and np-Ni indeed co-existed in the sample.

Thermal Dehydrogenation Characteristics of LiBH$_4$/np-Ni System

Figure 4 shows the temperature-programmed dehydrogenation curves of the LiBH$_4$/np-Ni (1:5) system and pristine LiBH$_4$. It can be seen that hydrogen release from the LiBH$_4$/np-Ni (1:5) system initiates at about 70°C and ends before 400°C, with ∼11.9 wt.% of hydrogen desorbed. In contrast, the starting dehydrogenation temperature is as high as 330°C for pristine LiBH$_4$, and only 3.5 wt.% of hydrogen can be released when heating to 500°C. Evidently, the thermal dehydrogenation stability of LiBH$_4$ was notably reduced by np-Ni. In addition, **Table 3** compares the dehydrogenation temperature of LiBH$_4$ supported on different
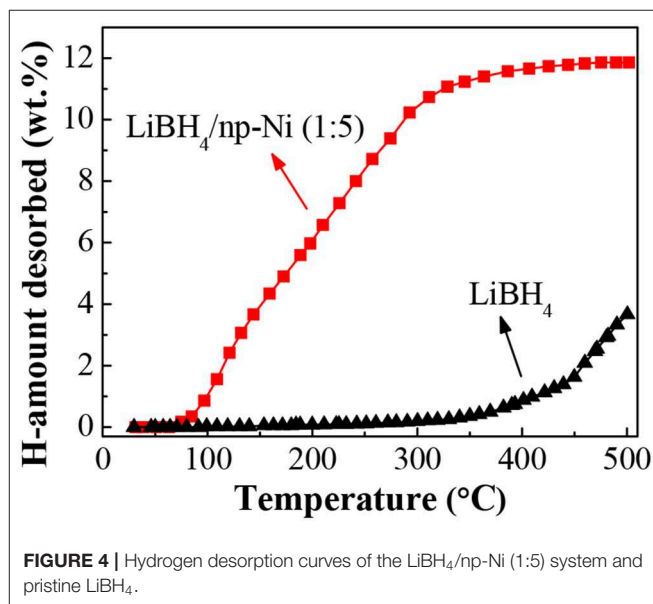
FIGURE 4 | Hydrogen desorption curves of the LiBH$_4$/np-Ni (1:5) system and pristine LiBH$_4$.

carriers. It is observed that the present LiBH$_4$/np-Ni (1:5) system has lower starting and ending dehydrogenation temperatures as compared with the reported LiBH$_4$-based supporting systems. In other words, np-Ni can provide a stronger destabilization effect on LiBH$_4$ relative to other carriers due to its synergistic effect of nanoconfinement and metallic catalysis. On the one hand, nanoconfinement of LiBH$_4$ in np-Ni can decrease the particle size to nanoscale level, which is very helpful to facilitate the dehydrogenation by enlarging the reaction interface and shortening the element diffusion distance. On the other hand, Ni itself can act as the dehydrogenation catalyst for LiBH$_4$ by enhancing charge donation ability of Li atom to BH$_4$ unit and thus weakening the B–H bond due to its high electronegativity.

To further monitor the dehydrogenation process, **Figure 5** gives the FTIR spectra of LiBH$_4$/np-Ni (1:5) systems after dehydrogenation at different temperatures. As can be seen

TABLE 3 | Hydrogen desorption temperature of LiBH$_4$ with different carriers.

Carriers	Starting temperature (°C)	Ending temperature (°C)	References
ZnO/ZnCo$_2$O$_4$	169	<500	Xu et al., 2017
CMK-3	220	<600	Zhang et al., 2007
Carbon aerogels@CoNiB	192	600	Zhao et al., 2014
SBA-15	150	>500	Ngene et al., 2010a
Single-walled carbon nanotubes	270	550	Fang et al., 2008a
Carbon nanotubes	250	<600	Yu et al., 2007
Nanoporous carbon	220	420	Liu et al., 2010
Nanoscale SiO$_2$	200	500	Chen et al., 2010
np-Ni	70	400	This work
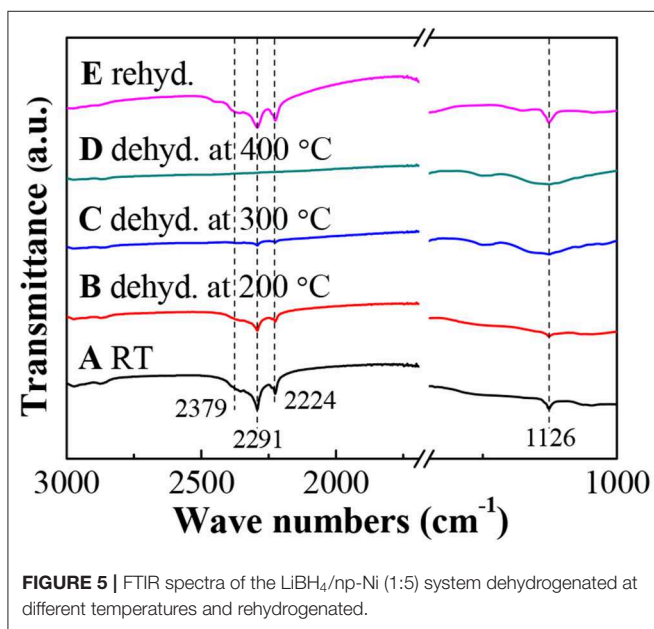
FIGURE 5 | FTIR spectra of the LiBH$_4$/np-Ni (1:5) system dehydrogenated at different temperatures and rehydrogenated.

in **Figure 5**A, the obvious characteristic bands for B–H bond vibrations located at 2,379, 2,291, 2,224 and 1,126 cm^{-1} (Zhang et al., 2011) confirm the existence of LiBH$_4$. With increasing the dehydrogenation temperature, the band intensity of B–H bond vibrations decreases gradually, indicating a continuous consumption of LiBH$_4$. Moreover, almost no FTIR bands can be observed in **Figure 5**D, which means that LiBH$_4$ was almost completely decomposed at 400°C. This result is in good agreement with the dehydrogenation phenomenon shown in **Figure 4**.

Dehydrogenation Kinetics of LiBH$_4$/np-Ni Systetm

Figure 6A presents the isothermal dehydrogenation curves of the LiBH$_4$/np-Ni (1:5) system at the temperatures of 250, 300, and

350°C, respectively. It is observed that the dehydrogenation rate increases as the temperature rises. For example, the amounts of hydrogen desorbed within 5 min are 7.3, 9.4, and 10.4 wt.% at 250, 300, and 350°C, respectively. In order to further reveal the dehydrogenation mechanism, the experimental dehydrogenation data were fitted by the kinetic modeling of $g(\alpha) = \int d\alpha/f(\alpha) = kt$, where α is the reacted fraction at time t, $g(\alpha)$ and $f(\alpha)$ are the functions representing different reaction mechanisms, and k is the rate constant (Li Y. et al., 2011; Liu D. M. et al., 2013). As the result, the function of -ln(1-α) gives the best linearity (see **Figure 6B**) over a broader α range for each measurement with the correlation coefficient of R^2 >0.99. This result indicates that dehydrogenation of the LiBH$_4$/np-Ni (1:5) system follows the first-order mechanism in the investigated temperature range.

According to the slope of the fitted straight line in **Figure 6B**, the k value at different temperatures can be obtained. Then the apparent activation energy for hydrogen desorption (E_a) can be determined based on the Arrhenius equation of $k = k_0 \cdot \exp[-E_a/(RT)]$, where k_0 is the pre-exponential factor, R is the gas constant, and T is the temperature. **Figure 6C** gives the Arrhenius plot for the LiBH$_4$/np-Ni (1:5) system. From the slope ($-E_a/R$) of the fitted straight line, E_a was calculated to be 11.4 kJ/mol. As reported in the literatures that E_a for LiBH$_4$ supported on CMK-3 and carbon aerogels@CoNiB are 40 and 46.39 kJ/mol, respectively (Zhang et al., 2007; Zhao et al., 2014). The lower E_a value for the present LiBH$_4$/np-Ni (1:5) system is originating from the synergistic effect of nanoconfinement and metallic catalysis of np-Ni, and can be regarded as one of the most important reasons for the enhanced dehydrogenation properties shown in **Figures 4**, **6A**. Moreover, the preparation process of np-Ni carrier for LiBH$_4$ by dealloying method is far more convenient than that of CMK-3 based on template method.

Rehydrogenation Characteristics of LiBH$_4$/np-Ni System

The dehydrogenated residue of the LiBH$_4$/np-Ni (1:5) system was subjected to rehydrogenation, and **Figure 7** demonstrates the isothermal rehydrogenation curve. It is observed that the LiBH$_4$/np-Ni (1:5) system can readily reabsorb 8.3 wt.% of hydrogen at 450°C under 8 MPa hydrogen pressure. The FTIR spectrum for the rehydrogenated product shown in **Figure 5**E suggests that LiBH$_4$ was regenerated. The inset of **Figure 7** gives the second hydrogen desorption curve of the LiBH$_4$/np-Ni (1:5) system. It can be seen that ∼8.2 wt.% of hydrogen can be released during the second dehydrogenation process. Note that the starting dehydrogenation temperature keeps in a low value of about 60°C. The result indicates undoubtedly that the synergistic effect of nanoconfinement and metallic catalysis of np-Ni maintains well upon repeated dehydrogenation/hydrogenation.

CONCLUSIONS

In order to improve the hydrogen storage properties of LiBH$_4$, the nanoporous Ni-based alloy was prepared by dealloying of the precursor Mn$_{70}$Ni$_{30}$ alloy and then used as the carrier to support LiBH$_4$ by wet impregnation method. It was found that the constructed LiBH$_4$/np-Ni (1:5) system can release ∼11.9
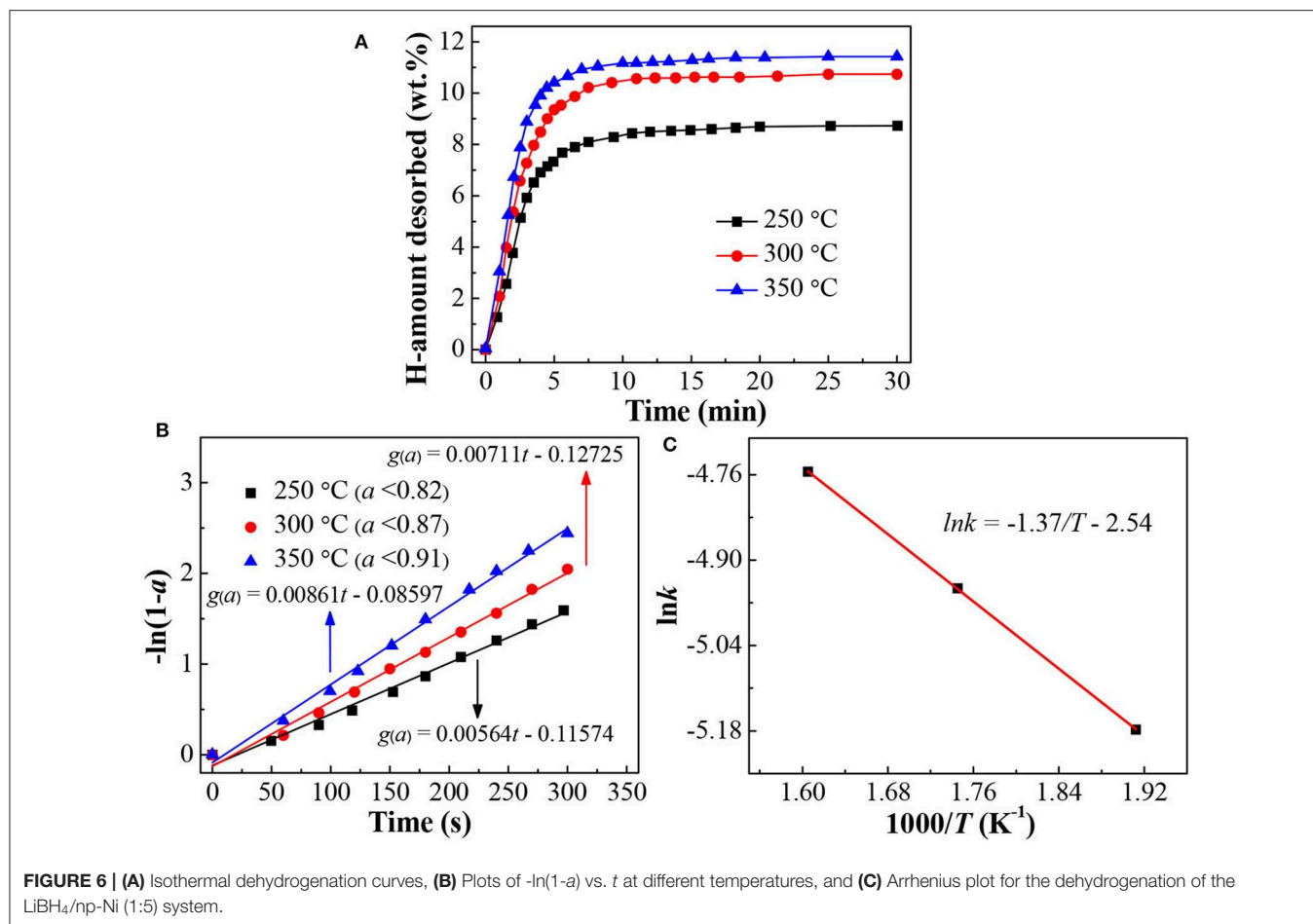
FIGURE 6 | (A) Isothermal dehydrogenation curves, **(B)** Plots of -ln(1-*a*) vs. *t* at different temperatures, and **(C)** Arrhenius plot for the dehydrogenation of the LiBH₄/np-Ni (1:5) system.
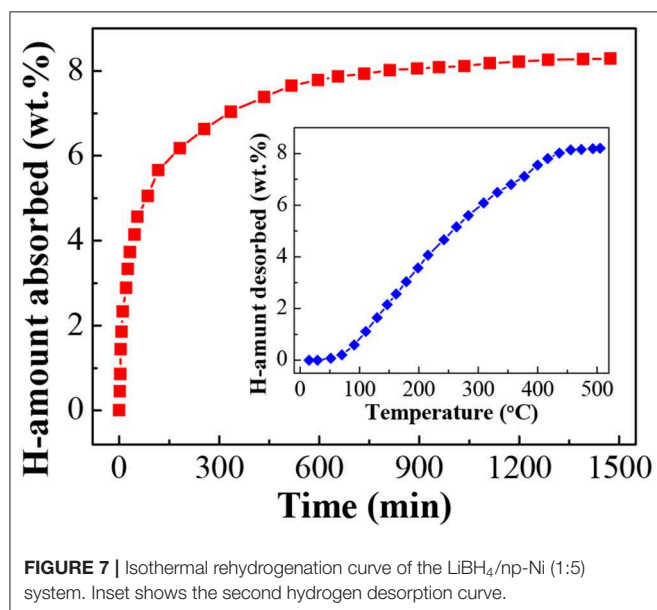
FIGURE 7 | Isothermal rehydrogenation curve of the LiBH₄/np-Ni (1:5) system. Inset shows the second hydrogen desorption curve.

wt.% of hydrogen with the starting and ending dehydrogenation temperatures as low as about 70 and 400°C, respectively. Due to the synergistic effect of nanoconfinement and metallic catalysis

of nanoporous Ni-based alloy, the apparent dehydrogenation activation energy of LiBH₄ was remarkable decreased to about 11.4 kJ/mol. The dehydrogenated residue can readily absorb hydrogen to regenerate LiBH₄ at 450°C under 8 MPa hydrogen pressure. Moreover, the starting dehydrogenation temperature keeps in a low value of about 60°C during the second dehydrogenation process.

DATA AVAILABILITY STATEMENT

All datasets generated for this study are included in the article.

AUTHOR CONTRIBUTIONS

XC and DL contributed conception and design of the study. XC and YZ were in charge of the analysis of data. ZL and CW prepared samples and performed characterization. All authors contributed to manuscript revision, read, and approved the submitted version.

FUNDING

REFERENCES

Abdalla, A. M., Hossain, S., Nisfindy, O. B., Azad, A. T., Dawood, M., and Azad, A. K. (2018). Hydrogen production, storage, transportation and key challenges with applications: a review. *Energ. Convers. Manage.* 165, 602–627. doi: 10.1016/j.enconman.2018.03.088

Abe, J. O., Popoola, A. P. I., Ajenifuja, E., and Popoola, O. M. (2019). Hydrogen energy, economy and storage: review and recommendation. *Inter. J. Hydr. Energy* 44, 15072–15086. doi: 10.1016/j.ijhydene.2019.04.068

Cai, R., Sun, L. X., Xu, F., Zou, Y. J., and Chu, H. L. (2016). LiBH$_4$ confined in nitrogen-doped ordered mesoporous carbons for hydrogen storage. *Mater. Sci. Forum* 852, 858–863. doi: 10.4028/www.scientific.net/MSF.852.858

Cai, W., Hou, J., Tao, P., and Yang, Y. (2018). An insight into the dehydrogenation behaviour of LiBH$_4$ exhibiting remarkable kinetics enhanced by nanostructured h-BN. *J. Alloy Compd.* 750, 443–450. doi: 10.1016/j.jallcom.2018.04.022

Chen, X. Y., Guo, Y. H., Gao, L., and Yu, X. B. (2010). Improved dehydrogenation of LiBH$_4$ supported on nanoscale SiO$_2$ via liquid phase method. *J. Mater. Res.* 25, 2415–2421. doi: 10.1557/JMR.2010.0301

Ding, Z., Wu, P., and Shaw, L. (2019). Solid-state hydrogen desorption of 2MgH$_2$ + LiBH$_4$ nano-mixture: a kinetics mechanism study. *J. Alloy Compd.* 806, 350–360. doi: 10.1016/j.jallcom.2019.07.218

Fang, Z. Z., Kang, X. D., Wang, P., and Cheng, H. M. (2008a). Improved reversible dehydrogenation of lithium borohydride by milling with as-prepared single-walled carbon nanotubes. *J. Phys. Chem. C* 112, 17023–17029. doi: 10.1021/jp803916k

Fang, Z. Z., Kang, X. D., Yang, Z. X., Walker, G. S., and Wang, P. (2011). Combined effects of functional cation and anion on the reversible dehydrogenation of LiBH$_4$. *J. Phys. Chem. C* 115, 11839–11845. doi: 10.1021/jp200137n

Fang, Z. Z., Wang, P., Rufford, T. E., Kang, X. D., Lu, G. Q., and Cheng, H. M. (2008b). Kinetic- and thermodynamic-based improvements of lithium borohydride incorporated into activated carbon. *Acta Mater.* 56, 6257–6263. doi: 10.1016/j.actamat.2008.08.033

Gasnier, A., Luguet, M., Pereira, A. G., Troiani, H., Zampieri, G., and Gennari, F. C. (2019). Entanglement of N-doped graphene in resorcinol-formaldehyde: Effect over nanoconfined LiBH$_4$ for hydrogen storage. *Carbon* 147, 284–294. doi: 10.1016/j.carbon.2019.02.090

Guo, L., Li, Y., Ma, Y., Liu, Y., Peng, D., Zhang, L., et al. (2017). Enhanced hydrogen storage capacity and reversibility of LiBH$_4$ encapsulated in carbon nanocages. *Inter. J. Hydr. Energy* 42, 2215–2222. doi: 10.1016/j.ijhydene.2016.11.184

Izumi, F., and Ikeda, T. (2000). A rietveld-analysis programm RIETAN-98 and its applications to zeolites. *Mater. Sci. Forum* 321–324, 198–205. doi: 10.4028/www.scientific.net/MSF.321-324.198

Li, C., Peng, P., Zhou, D. W., and Wan, L. (2011). Research progress in LiBH$_4$ for hydrogen storage: a review. *Inter. J. Hydrogen Energy* 36, 14512–14526. doi: 10.1016/j.ijhydene.2011.08.030

Li, H. W., Yan, Y. G., Orimo, S., Züttel, A., and Jensen, C. M. (2011). Recent progress in metal borohydrides for hydrogen storage. *Energies* 4, 185–214. doi: 10.3390/en4010185

Li, Y., Zhou, G., Fang, F., Yu, X., Zhang, Q., Ouyang, L., et al. (2011). De-/re-hydrogenation features of NaAlH$_4$ confined exclusively in nanopores. *Acta Mater.* 59, 1829–1838. doi: 10.1016/j.actamat.2010.11.049

Liu, D. M., Huang, W. J., Si, T. Z., and Zhang, Q. A. (2013). Hydrogen storage properties of LiBH$_4$ destabilized by SrH$_2$. *J. Alloy Compd.* 551, 8–11. doi: 10.1016/j.jallcom.2012.09.138

Liu, D. M., Tan, Q. J., Gao, C., Sun, T., and Li, Y. T. (2015). Reversible hydrogen storage properties of LiBH$_4$ combined with hydrogenated Mg$_{11}$CeNi alloy. *Inter. J. Hydr. Energy* 40, 6600–6605. doi: 10.1016/j.ijhydene.2015.03.130

Liu, H., Wang, X., Zhou, H., Gao, S., Ge, H., Li, S., et al. (2016). Improved hydrogen desorption properties of LiBH$_4$ by AlH$_3$ addition. *Inter. J. Hydrogen Energy* 41, 22118–22127. doi: 10.1016/j.ijhydene.2016.09.177

Liu, X. F., Peaslee, D., Jost, C. Z., and Majzoub, E. H. (2010). Controlling the decomposition pathway of LiBH$_4$ via confinement in highly ordered nanoporous carbon. *J. Phys. Chem. C* 114, 14036–14041. doi: 10.1021/jp1055045

Liu, Y., Heere, M., Vasquez, L. C., Paterakis, C., Sørby, M. H., Hauback, B. C., et al. (2018). Dehydrogenation and rehydrogenation of a 0.62LiBH$_4$-0.38NaBH$_4$ mixture with nano-sized Ni. *Inter. J. Hydrogen Energy* 43, 16782–16792. doi: 10.1016/j.ijhydene.2018.04.211

Lowell, S., Shields, J. E., Thomas, M. A., and Thommes, M. (2004). *Characterization of Porous Solids and Powders: Surface Area, Pore Size and Density*. Dordrecht: Springer.

Mauron, P., Buchter, F., Friedrichs, O., Remhof, A., Bielmann, M., Zwicky, C. N., et al. (2008). Stability and reversibility of LiBH$_4$. *J. Phys. Chem. B* 112, 906–910. doi: 10.1021/jp077572r

Meng, X., Wan, C., Wang, Y., and Ju, X. (2018). Porous Ni@C derived from bimetallic metal-organic frameworks and its application for improving LiBH$_4$ dehydrogenation. *J. Alloy Compd.* 735, 1637–1647. doi: 10.1016/j.jallcom.2017.11.191

Ngene, P., Adelhelm, P., Beale, A. M., de Jong, K. P., and de Jong, P. E. (2010a). LiBH$_4$/SBA-15 nanocomposites prepared by melt infiltration under hydrogen pressure: synthesis and hydrogen sorption properties. *J. Phys. Chem. C* 114, 6163–6168. doi: 10.1021/jp9065949

Ngene, P., van Zwienen, M. R., and de Jongh, P. E. (2010b). Reversibility of the hydrogen desorption from LiBH$_4$: a synergetic effect of nanoconfinement and Ni addition. *Chem. Commun.* 46, 8201–8203. doi: 10.1039/c0cc03218b

Ngene, P., Verkuijlen, M. H., Zheng, Q., Kragten, J., Bentum, P. J. M., Bitter, J. H., et al. (2011). The role of Ni in increasing the reversibility of the hydrogen release from nanoconfined LiBH$_4$. *Faraday Discuss.* 151, 47–58. doi: 10.1039/C0FD00028K

Orimo, S., Nakamori, Y., Kitahara, G., Miwa, K., Ohba, N., Towata, S., et al. (2005). Dehydriding and rehydriding reactions of LiBH$_4$. *J. Alloy Compd.* 404, 427–430. doi: 10.1016/j.jallcom.2004.10.091

Shao, J., Xiao, X., Fan, X., Huang, X., Zhai, B., Li, S., et al. (2015). Enhanced hydrogen storage capacity and reversibility of LiBH$_4$ nanoconfined in the densified zeolite-templated carbon with high mechanical stability. *Nano Energy* 15, 244–255. doi: 10.1016/j.nanoen.2015.04.023

Sun, W. W., Li, S. F., Mao, J. F., Guo, Z. P., Liu, H. K., Dou, S. X., et al. (2011). Nanoconfinement of lithium borohydride in Cu-MOFs towards low temperature dehydrogenation. *Dalton Trans.* 40, 5673–5676. doi: 10.1039/c0dt01727b

Surrey, A., Minella, C. B., Fechler, N., Antonietti, M., Grafe, H. J., Schultz, L., et al. (2016). Improved hydrogen storage properties of LiBH$_4$ via nanoconfinement in micro-and mesoporous aerogel-like carbon. *Inter. J. Hydr. Energy* 41, 5540–5548. doi: 10.1016/j.ijhydene.2016.01.163

Xu, X. H., Zang, L., Zhao, Y. R., Zhao, Y., Wang, Y. J., and Jiao, L. F. (2017). Hydrogen storage behavior of LiBH$_4$ improved by the confinement of hierarchical porous ZnO/ZnCo$_2$O$_4$ nanoparticles. *J. Power Sources* 359, 134–141. doi: 10.1016/j.jpowsour.2017.05.047

Yang, J., Sudik, A., Wolverton, C., and Siegel, D. J. (2010). High capacity hydrogen storage materials: attributes for automotive applications and techniques for materials discovery. *Chem. Soc. Rev.* 39, 656–675. doi: 10.1039/b802882f

Yin, L., Wang, P., Fang, Z., and Cheng, H. (2008). Thermodynamically tuning LiBH$_4$ by fluorine anion doping for hydrogen storage: a density functional study. *Chem. Phys. Lett.* 450, 318–321. doi: 10.1016/j.cplett.2007.11.060

Yu, X. B., Wu, Z., Chen, Q. R., Li, Z. L., Weng, B. C., and Huang, T. S. (2007). Improved hydrogen storage properties of LiBH$_4$ destabilized by carbon. *Appl. Phys. Lett.* 90:034106. doi: 10.1063/1.2432240

Zhang, B. J., Liu, B. H., and Li, Z. P. (2011). Destabilization of LiBH$_4$ by (Ce, La)(Cl, F)$_3$ for hydrogen storage. *J. Alloy Compd.* 509, 751–757. doi: 10.1016/j.jallcom.2010.09.066

Zhang, L., Zheng, J., Xiao, X., Wang, X., Huang, X., Liu, M., et al. (2017). A new strategy to remarkably improve the low-temperature reversible hydrogen desorption performances of LiBH$_4$ by compositing with fluorographene. *Inter. J. Hydr. Energy* 42, 20046–20055. doi: 10.1016/j.ijhydene.2017.05.060

Zhang, Y., Liu, Y., Yang, Y., Li, Y., Hu, J., Gao, M., et al. (2018). Superior catalytic activity of in situ reduced metallic Co for hydrogen storage in a Co(OH)$_2$-containing LiBH$_4$/2LiNH$_2$ composite. *Mater. Res. Bull.* 97, 544–552. doi: 10.1016/j.materresbull.2017.09.037

Zhang, Y., Zhang, W. S., Wang, A. Q., Sun, L. X., Fan, M. Q., Chu, H. L., et al. (2007). LiBH₄ nanoparticles supported by disordered mesoporous carbon: Hydrogen storage performances and destabilization mechanisms. *Inter. J. Hydr. Energy* 32, 3976–3980. doi: 10.1016/j.ijhydene.2007.04.010

Zhao, Y. P., Jiao, L. F., Liu, Y. C., Guo, L. J., Li, L., Liu, H. Q., et al. (2014). A synergistic effect between nanoconfinement of carbon aerogels and catalysis of CoNiB nanoparticles on dehydrogenation of LiBH₄. *Inter. J. Hydr. Energy* 39, 917–926. doi: 10.1016/j.ijhydene.2013.10.137

Züttel, A., Rentsch, S., Fischer, P., Wenger, P., Sudan, P., Mauron, P.h., et al. (2003). Hydrogen storage properties of LiBH₄. *J. Alloy Compd.* 356, 515–520. doi: 10.1016/s0925-8388(02)01253-7